Annu. Rev. Phys. Chem. 1998. 49:337–69

PROTON-COUPLED ELECTRON TRANSFER

Robert I. Cukier
Department of Chemistry, Michigan State University, East Lansing, Michigan 48824-1322; e-mail: cukier@argus.cem.msu.edu

Daniel G. Nocera
Department of Chemistry, Massachusetts Institute of Technology, Cambridge, Massachusetts 02139-4307; e-mail: nocera@mit.edu

KEY WORDS: electron transfer, proton transfer, bionergetics, molecular dynamics, tunneling

ABSTRACT

Proton-coupled electron transfer (PCET) is an important mechanism for charge transfer in a wide variety of systems including biology- and materials-oriented venues. We review several areas where the transfer of an electron and proton is tightly coupled and discuss model systems that can provide an experimental basis for a test of PCET theory. In a PCET reaction, the electron and proton may transfer consecutively (ET/PT) or concertedly (ETPT). The distinction between these processes is formulated, and rate-constant expressions for the two reaction channels are presented. Methods for the evaluation of these rate constants are discussed that are based on dielectric continuum theory. Electron donor hydrogen-bonded-interface electron acceptor systems displaying PCET reactivity are presented, and the rate-constant expressions corresponding to the ETPT and ET/PT channels for several model reaction complexes are evaluated.

INTRODUCTION

The coupled transfer of electrons and protons is an important pathway of charge transport in a variety of biochemical, electrochemical, and small-molecule organic and inorganic reactions. The proteins and enzymes of photosynthesis and respiration have optimized structures that derive their function by utilizing energy gathered along a charge-separating network to drive a proton pump, which in turn is manifested in a transmembrane chemical potential that provides

0066-426X/98/1001-0337$08.00

the energy for the synthesis of complex biomolecules (1–9). The quintessential electrochemical process of hydrogen-ion discharge at an electrode must involve a coupled electron and proton transfer (10, 11). Recent developments in supramolecular solid-state chemistry are directed toward rational design of coupled electron proton transfer systems with novel electronic or photonic material properties (12–14). Here, photoinduced electron transfer induces proton transfer to promote a stable product.

In this review, we outline our recent theoretical (15–18) and experimental (19–24) efforts aimed at a systematic study of the coupling between proton and electron transfer, which we refer to as proton-coupled electron transfer (PCET). The work has been directed toward understanding PCET in biomimetic systems, where the potential for this coupling can be assessed in a systematic manner. Naturally, these studies are also relevant to nonbiological PCET systems. The compounds displayed in Figure 1 (20, 21) exemplify an experimental design tailored toward this investigation.

The electron donor and acceptor are separated by a hydrogen-bonded interface. Photochemical initiation of the electron transfer reaction between the donor (e.g. Ru-bipy) and the acceptor (e.g. dinitrobenzene) may result in the transfer of a proton that, as indicated in Figure 1, results in a large charge change in the interface. These studies permit important PCET questions to be explored, such as the following: (*a*) What factors distinguish the consecutive process of electron transfer (ET) followed by proton transfer (PT) from a concerted transfer of an electron and a proton (ETPT)? (*b*) What structural/electronic features of the proton interface are important in governing the coupling between the electron and the proton? (*c*) How will the energetics (e.g. reorganization and free energy) for charge transfer in an ET or PT reaction be different in PCET? (*d*) How will the PCET rate compare in magnitude with ET and PT rates?

We first discuss several examples of biological PCET that motivate the study of PCET in biomimetic compounds. PCET studies can be divided into those that address "physical" protons (those involved in translocation) and "chemical" protons (those needed for redox chemistry) (5, 25). Our focus is on the chemical protons that are tightly bound via hydrogen bonds to moieties that interact with electron transfer donors and acceptors (although, typically, later stages will involve the physical protons). An important PCET example is the photosystem II oxygen evolving complex (PSII/OEC), whose function is to split water (3). In bacterial reaction centers, the light-induced two-electron reduction of a quinone, Q_B, is coupled to proton transfer that ultimately leads to release of protons across the membrane to provide a transmembrane chemical potential (26). Extensive efforts have been under way to resolve this overall two-electron process into its elementary steps of proton and electron transfer (1, 2, 27–29). Two quinones are involved: a tightly bound, primary quinone designated Q_A, and

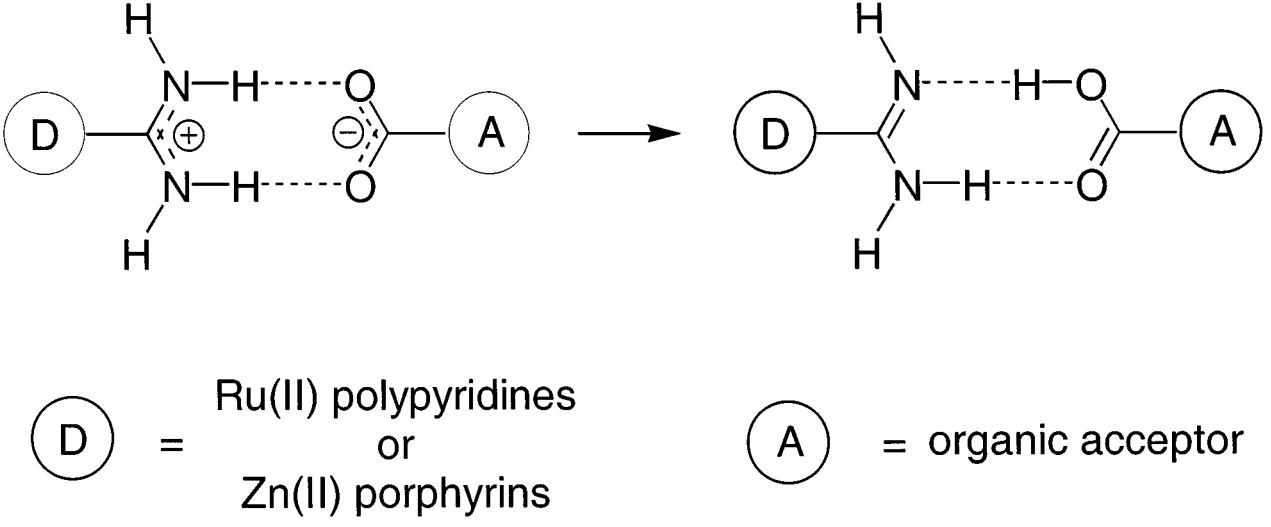

Figure 1 Compounds for PCET studies. The hydrogen-bonded interface exhibits substantial charge displacement with proton transfer.

a loosely bound, secondary quinone, Q_B. The reaction of the second electron is tightly coupled to the proton, schematically $(Q_A^- Q_B^-) + H^+ \rightarrow Q_A(Q_B H^-)$, and can be formulated as ET followed by PT or vice versa, or as a concerted transfer (30–32). An attempt has been made to infer the reaction pathway by inserting Q_A's of differing driving force into the reaction center, and it was concluded that PT occurs first and is followed by a rate-limiting ET step (33). PCET also plays a crucial role at the terminus responsible for oxygen evolution (3, 34). The OEC is linked to $P680^+$ by a redox-active tyrosine, Y_Z, which functions as a charge transfer interface, allowing productive forward electron transfer reactions to compete successfully with the wasteful but thermodynamically favorable charge recombination reaction in the RC (3, 35, 36). Results by Meyer et al (34) reveal that the protonation state of an acid-base group influences the kinetics of the $Y_Z P680^+ \rightarrow Y_Z^+ P680$ reaction, which are consonant with Lavergne & Junge's (37) results showing that proton release is coupled to the oxidation of Y_Z. EPR and ENDOR have verified that the oxidation of the tyrosine interface is closely coupled to proton transfer, but the mechanistic details of this PCET process remain elusive for Y_Z (38, 39). Another tyrosine, Y_D, symmetrically disposed relative to Y_Z, has been shown to be hydrogen bonded to a nearby histidine residue. The tryrosine is oxidized to a tyrosyl radical and re-reduces $P680^+$ to P680. The proton in the tyrosyl-histidine hydrogen bond transfers from the phenol to the nitrogen of the base (3, 38). This combination of ET to form the tyrosyl radical and PT from the phenol to the histidine comprises a tightly coupled PCET system amenable to the type of analysis carried out below (18). In addition, PCET is not limited to charge transport at this terminus of the photosystem; it has been proposed that the oxidation of water at the oxygen-evolving complex (OEC) proceeds by a series of PCET reactions of an oxo-bridged cluster of manganese (40). Consistent with this proposition is the marked pH dependence of the redox potential of OEC model oxo-manganese clusters (41, 42). Careful and complete kinetic isotope effect studies by Meyer and co-workers on ruthenium-oxo dimers led to the conclusion that such reaction mechanisms involve simultaneous transfer of an electron and proton (43–46). We mention in passing the extensive studies of PCET in cytochrome *c* oxidase, where, for example, the rate of electron transfer from the heme a^{2+} to heme a_3^{3+} is evidently proton coupled via interaction with a protonatable group close to the binuclear center (7, 8, 25, 47, 48). The role of proton influence on electron transfer in cytochrome *c* oxidase has recently been reviewed (9). Complexes between the nucleic acids in DNA and aromatic fluorophores exhibit strong fluorescence quenching of the latter by photoinduced electron transfer (49, 50). The electron transfer quenching in aqueous medium is proton coupled, as inferred from isotope effects and the lack of quenching in nonaqueous solvent (50). The proton comes from the hydrogen bonding

solvent, but the microscopic steps are difficult to elucidate, because the solvent contributes the proton. Molecular triads consisting of carotenoid–porphyrin–quinone (C–P–Q) triads have been designed with the goal of high quantum yield photochemically induced charge separation to $C^{\cdot+}$–P–$Q^{\cdot-}$ (51–53). A recent synthetic design incorporates an intramolecular hydrogen bond from a carboxylic acid group to the quinone carbonyl (54). ET from the excited porphyrin results in a large increase in the pK_a of the quinone. The consequent PT to the quinone carbonyl reduces the recombination rate and leads to a doubling of the quantum yield relative to the cognate nonhydrogen-bonded triads. Thus, for these triads, PT has a demonstrable effect on an ET reaction rate.

PCET is not confined to the biological arena, of course. Hydrogen ion discharge on a metal surface, schematized as $H_3O^+ + e^-(\text{Metal}) = H_{ads} + H_2O$, entails electron transfer from the metal with concomitant proton motion toward the electrode surface (11, 55, 56). A recent theoretical article analyzed this reaction with some concepts similar to those we introduce in the next section and is based on the idea that the electron and proton transfer together (57). Two complicating features of this electrode reaction are the requirement of averaging the rate constant over the Fermi level of the electron in the metal (as in conventional electron transfer reaction treatments of electrochemical processes) (10) and the difficulties engendered by the H_3O^+ not being a fixed distance from the electrode. An emergent theme in solid state materials chemistry is the synthesis of polymeric supramolecular structures (14) with the goal of creating switchable materials. Recently, donor–acceptor dimers, capable of undergoing photoinitiated electron transfer, were shown to form a polymeric supramolecular structure held together by hydrogen bonds between the donor of one and the acceptor of another of the dimeric species (58). Upon optical excitation, charge transfer to form a radical ion-pair state with subsequent proton transfer in the hydrogen bond was postulated where the proton transfer step is required to stabilize the ion pair. Thus, electron transfer leads to proton transfer in these materials. Two dimensional hydrogen bonded networks of quinhydrones have been synthesized (59). These H-bonded charge transfer complexes undergo electron and proton transfer, as inferred from the electronic spectrum of the product, but without kinetic studies the mechanism cannot be assessed.

The desire to explore PCET in a well-defined geometry motivated the synthesis of model compounds that preserve the features of charge separating networks in biological systems and permit the interrogation of the electron and proton dynamics (19–24). The key to the approach is to photoinduce electron transfer within a fixed-distance donor/acceptor pair that has a proton transfer network internal to the electron transfer pathway. The electron transfer kinetics is defined by color changes associated with the donor/acceptor chromophores, as monitored by time-resolved picosecond laser techniques. This approach is

analogous to the progression in studies of ET reaction dynamics, where the original bimolecular reaction kinetic studies were difficult to interpret because of reaction at varying donor-acceptor distances, the necessity of evaluation of the energetics of the precursor and successor complexes, and interference from diffusion control for fast ET (60). This motivated the design of intramolecular ET systems, where the donor-acceptor distance is fixed and controllable, the energetics are specific to the ET step, and diffusion is not an issue (61, 62). With the advent of photochemical initiation of ET (47), fast ET events could then be interrogated without the risk of a switchover to diffusion control of the reaction kinetics. This design for PCET follows a similar strategy, with a similar rationale.

From the perspective of theory, fixing the geometry of the ET and PT donor and acceptors greatly simplifies the analysis. Averages over varying donor-acceptor distances do not have to be carried out, and since the reaction is intramolecular, the energetics are determined by the donor-acceptor hydrogen bonded complex's interaction with the solvent. The number of parameters that need to be evaluated once a rate expression is obtained is then greatly restricted relative to what would be required for a treatment of a bimolecular process. Then, the available theories for unimolecular ET and PT can be used as a framework with which to construct a PCET theory for consecutive reaction steps, and the construction of a theory for concerted ETPT does not suffer from such complications.

THEORY OF PCET REACTIONS

In this section, we provide a theory for PCET in donor-acceptor complexes as exemplified in Figure 1. Our initial efforts were devoted to a description of PCET in symmetric interfaces (15, 16), as experimentally realized by dicarboxylic acid hydrogen bonded interfaces (19). The asymmetric interfaces are of greater interest, as they are much more common in nature, and furthermore, the theory of asymmetric interfaces (17, 18) can of course be reduced to that of a symmetric interface by specialization. Thus, in this section, we restrict the discussion to asymmetric interfaces. The symmetric interface theory is summarized below, where the experimental results on carboxylic acid dimer interfaces are discussed.

A key issue is the mechanism of the net reaction that transfers an electron and a proton from an initial state to a final state where both the electron and proton have transferred. In other words, the electron transfer's "function" is to transfer a proton. There are two, competitive, channels leading to both the electron and proton transferring. One channel is a *consecutive* process, with electron transfer (ET) followed by proton transfer (PT). This process is referred to as ET/PT,

the slash denoting the consecutivity of the process. (We assume that ET occurs first, as the experimental design discussed here initiates ET photochemically. In any case, the process of PT followed by ET can be discussed, formally, in similar fashion to ET/PT.) Let us stress that the electron transfer may or may not stimulate the proton transfer. Upon electron transfer, the proton may be thermodynamically and/or kinetically prompted to transfer as the electronic energy and solvation energetics that the proton experiences will typically be different after the ET reaction. That is, the potential energy surface (pes) governing the proton transfer may become favorable for proton transfer after the electron transfer. Thermodynamically, the proton may exhibit a lower pK_a after ET. But to predict kinetics, the driving force of the reaction, $\Delta G^{(0)}$, is not sufficient. For proton transfer reactions whose mechanism can be formulated through Marcus-Levich theory, there will be a reorganization energy λ_s contribution to the rate expression, and this is a nonequilibrium quantity (10, 11, 56, 63, 64). That ET may stimulate PT is a feature analogous to excited state proton transfer reactions (photoacids) where, upon electronic excitation, a proton may become much more labile (65). Here, it is the electron transfer that may act like an electronic excitation in the sense of inducing a proton transfer reaction.

In ET/PT there are two quantum events: electron tunneling and proton tunneling. These tunneling events are both induced by solvent fluctuations. (Contributions from bond rearrangements can also occur upon the electron transfer, but in many reactions, solvation energetics is dominant). For electron transfer, the Marcus-Levich picture is schematized in Figure 2, from the point of view of the electron coordinate (r_e) and the solvent coordinate (R).

The solvent fluctuates to a configuration where the electron's energy on the donor (D) and acceptor (A) are essentially equal. At this "transition state" configuration, the electron can tunnel through the potential barrier and then, via further solvent fluctuations, be stabilized in the product state. The solvent coordinate figure is obtained by expressing the Hamiltonian consisting of the terms for the electron, its interaction with the solvent, and the solvent's energy in a two-state basis of localized (initial and final) states. The diabats for the initial electron state, *i*, and the final electron state, *f*, are drawn in Figure 2*b*. Including the off-diagonal coupling, responsible for the charge transfer, produces adiabatic surfaces that split the diabats in the region of their crossing. The separation between the two (symmetric and antisymmetric) eigenfunctions is twice the electronic coupling matrix element V_{el} (shown in Figure 2*a*). It represents the electronic overlap of the wavefunctions on donor and acceptor. In a simplest ET picture, then, the rate will be determined by this electronic overlap, and the activation energy defined as the fraction of all solvent configurations that correspond to this transition state, R^*, as indicated on Figure 2. When the electronic coupling is weak, the nonadiabatic limit of ET is appropriate and the

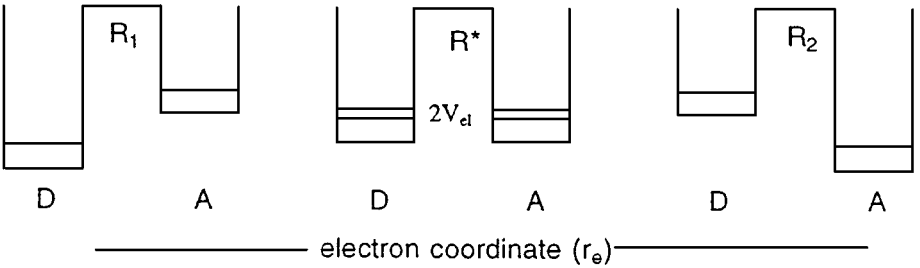

(a)

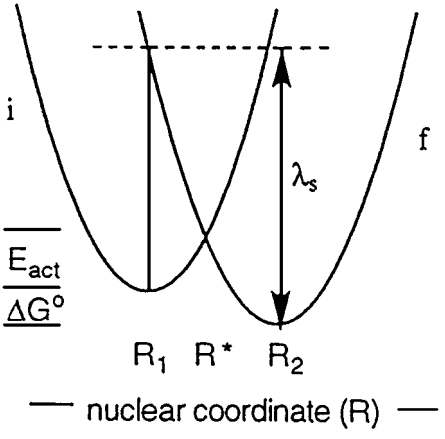

(b)

Figure 2 (*a*) Electronic energy surfaces for an ET reaction. The three surfaces correspond to solvent configurations R_1 (R^*) [R_2] with the electron in its initial (transition) [final] state. With the solvent at R^*, the electron may transfer. (*b*) Marcus solvation (nuclear) coordinate for an ET reaction.

rate constant is given by (10, 56)

$$k_{ET} = \frac{V_{el}^2}{\hbar^2}\sqrt{\pi\hbar^2/\lambda_s k_B T}\, e^{-(\lambda_s+\Delta G^{(0)})^2/4\lambda_s k_B T}. \qquad 1.$$

The Marcus form of the activation energy above is obtained by a classical treatment of the solvent (its characteristic frequencies should be small compared with k_BT), and the assumption that the solvation surfaces are quadratic. The latter assumption is a consequence of the assumed linear response of the solvent to the presence of the charge distribution of the solute.

Proton transfer reactions can be thought of in similar fashion (11, 56, 66). However, it must be stressed that there are other mechanisms for a proton transfer reaction (67). We assume here that the proton transfer mechanism is the same as that for electron transfer. Weaker H bonds favor this circumstance, indicating a substantial barrier between the initial and final states. An expression analogous to Equation 1 may be used for k_{PT}. We denote the proton's initial state as *a* and final state, when it has transferred, as *b*.

The consecutive mechanism is distinct from another pathway for the overall conversion: a *concerted* process whereby the electron and the proton transfer during the same tunneling event. In this case, a given solvent fluctuation produces a state with a significant probability for the electron and proton to transfer together. We refer to this process as ETPT. We have formulated an approach to ETPT that is analogous to that outlined above for ET or PT and refer to it as the two-dimensional (2D) approach (17). In this method, the electron and the proton are treated on the same footing in a 2D tunneling space, where the energy levels are those of the proton and electron, and these levels are parametric on the solvent configuration. It is a generalization of the ET mechanism sketched above. With this approach, we may obtain a qualitative picture of the ingredients that lead to ET/PT or to ETPT. A suitable potential energy function for this discussion is

$$V(r_e, r_p \mid R) = V(r_e) + V(r_p) + \gamma r_e r_p + c_e r_e R + c_p r_p R + \frac{1}{2} k_s R^2. \qquad 2.$$

The terms on the right side of Equation 2 represent, respectively, the isolated transfer-electron's pes with r_e, the electron's coordinate; the isolated transfer-proton's pes with r_p, the proton's coordinate; a coupling between the electron and proton with strength γ, the coupling between the solvent, with coordinate *R*, and the electron (proton), with strength $c_e(c_p)$; and the solvent's contribution to the energetics with k_s, the solvent force constant. In the absence of the electron proton coupling term ($\gamma = 0$), the Hamiltonian based on Equation 2 would be separable and each part would lead, in the two-state basis approach discussed above, to the charge transfer mechanism schematized by Figure 2. The use of a harmonic approximation for the solvent is familiar from dielectric theory where the appropriate coordinate is the solvent's orientational polarization (63, 68). With suitable interpretation of the force constant, it is Marcus's reaction coordinate. The transfer electron's and proton's potentials can be thought of as symmetrical double-well potentials with minima at $-r_{eo}(+r_{eo})$ for the $i(f)$ state and at $-r_{po}(+r_{po})$ for the proton $a(b)$ state. The coupling γ between the electron and proton serves as an electronic structure effect whereby the electron transfer reaction may make proton transfer more favorable thermodynamically. For example, if γ were negative, electron transfer

would be endothermic and the subsequent proton transfer exothermic, while the ETPT event would be thermoneutral. The functional form of the interaction is not of significance. Whether this coupling does enhance PT upon ET or enhances ETPT will also depend on the solvation energetics of the corresponding reaction. The terms proportional to c_e (c_p) provide the effect of the solvation coupling to the electron (proton) that can symmetrize the pes to permit electron, proton, or electron-proton transfer. In the contribution $c_p r_p R$, r_p may be regarded as the dipole moment operator of the proton that changes as the proton transits from its initial to final state; R would then be the fluctuating electric field from the solvent, and c_p would determine the strength of the coupling. A dipole-electric field coupling is quite reasonable as a model that captures the major effect of a polar solvent on the transferring proton (69).

To investigate the analog of the solvent surfaces for electron transfer shown in Figure 2, we may use a four-state basis, where the basis functions consist of electron and proton initial and final states (localized in the respective reactant and product wells for both the electron and the proton). In this localized-state basis (not the eigenstates of H), the four energies that are parametrically dependent on the solvent coordinate R correspond are the following diabatic surfaces:

$$
\begin{aligned}
E_{ia} &= \frac{1}{2}k_s(R - R_{ia})^2 + \gamma d_e d_p; \quad R_{ia} = (c_s d_s + c_p d_p)/k_s, \\
E_{ib} &= \frac{1}{2}k_s(R - R_{ib})^2 - \gamma d_e d_p; \quad R_{ib} = (c_s d_s - c_p d_p)/k_s, \\
E_{fa} &= \frac{1}{2}k_s(R - R_{fa})^2 - \gamma d_e d_p; \quad R_{fa} = (-c_s d_s + c_p d_p)/k_s, \\
E_{fb} &= \frac{1}{2}k_s(R - R_{fb})^2 + \gamma d_e d_p; \quad R_{fb} = (-c_s d_s - c_p d_p)/k_s.
\end{aligned}
\tag{3.}
$$

The quantities $\pm d_s$ ($\pm d_p$) are the expectation values of the operators $\pm r_s$ ($\pm r_p$) in the two localized states, i and f for the electron (a and b for the proton). They essentially are equal to the spatial locations of the two charges in their possible states; at $-r_{eo}$ ($+r_{eo}$) for the electron i (f) states and at $-r_{po}$ ($+r_{po}$) for the proton a (b) states introduced above. The location of the minima on each surface, the quantities R_{ia} and the like, are obtained by minimizing the four surface's energies with respect to the solvent coordinate R. In this representation, the coupling that permits transfer of charge will consist of offdiagonal elements that can be viewed as constants. (Diagonalization of the resulting 4×4 Hamiltonian would lead to the adiabatic surfaces, but it seems clearer to use the diabats, in analogy to the charge-transfer picture of Figure 2.) A plot of the four diabatic surfaces that are obtained in this manner is shown in Figure 3*a*, where we have chosen γ as a negative number to indicate an

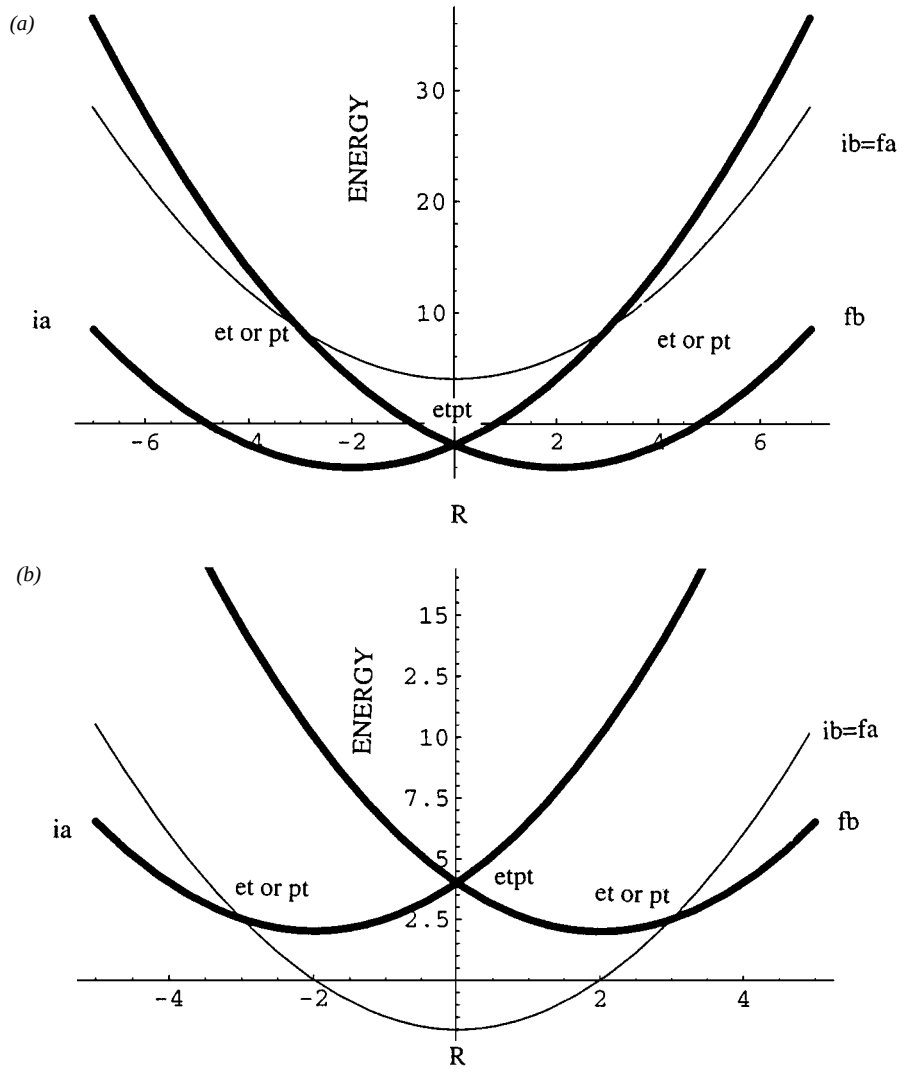

Figure 3 (*a*) Diabatic surfaces for ET/PT and ETPT. ETPT is favored because the activation energy for going along the *ia* surface to cross to the *fb* surface at $R = 0$ is the smallest here. ET (PT) corresponds to going along the *ia* surface, not crossing at zero, but crossing at the *fa* (*ib*) intersection. The *ib* and *fa* surfaces are degenerate because of symmetry. (*b*) Diabatic surfaces for ET/PT and ETPT. ET (or PT) is favored relative to ETPT, as can be seen by starting in the minimum of the *ia* surface and noting the small activation energy for the crossing to the left to the *ib* (or *fa*) surface relative to the activation for crossing to the right onto the *fb* surface.

attractive interaction between the electron and proton. That destabilizes the ET and PT pathways relative to the ETPT pathway.

We have assumed that the first two terms on the right side of Equation 3 represent symmetric double wells to construct this picture. The crossing at $R = 0$ of the *ia* and *fb* surfaces of energy E_{ia} and E_{fb}, respectively, indicates that for this value of R there is an energy degeneracy where the electron and proton may transfer as one quantum event. The probability of this crossing depends on the strength of the coupling, offdiagonal elements of the H in this diabatic basis. Thus, it is also possible to *not* cross from the *ia* to the *fb* surface and instead continue along the *ia* surface to cross to the *ib* surface (PT) or to the *fa* surface (ET). (Because of the maximal symmetry of this simple example, the *ib* and *fa* surfaces are coincident.) The activation energy for these latter processes are considerably higher than for the ETPT process. A less schematic view of the possible pathways for PCET has been explored by direct diagonalization of a Hamiltonian similar to the one in Equation 2 (70–72).

Note that R is a fluctuating quantity, of course, and this figure must be understood as an exploration of the energy of the various surfaces as a function of the solvent configuration; that is, it is not a diagram of a gas-phase trajectory for the solvent. Of course, the system does start in a definite state—here, the equilibrium (minimum) on the *ia* surface, as prepared by the photochemical excitation. Figure 3*b* is the same as for Figure 3*a* but with γ positive. Now it is ET or PT that is favored relative to ETPT, as seen by starting in the minimum of the *ia* surface and noting the small activation energy for the crossing to the left. Finally, if we introduce an exothermicity to the final-state surface, indicating a driving force for the overall conversion to the final states, *f* and *b*, then the four levels can look as in Figure 4. Here, the ETPT reaction is essentially activationless and, other things being equal, would proceed at a faster rate than either ET or PT.

The above simple construction shows that ET/PT and ETPT are competing reaction channels. In part, which channel is favored depends on the activation energy of the process. But, it also depends on the strength of the electronic coupling between the surfaces that are involved.

The above discussion treats the electron and proton on an equal footing, and this is useful for exploring the mechanism of ETPT. However, a proton is a much less quantum mechanical object than an electron. The implication is that while it is certainly appropriate to only consider two states for the electron, essentially ground states of the initial and final localized electron states, that is not the case for a proton. There is a manifold of localized proton states on the initial side, and a corresponding manifold of states on the final side. While the proton initial states may not be thermally accessible, as the proton well frequency is about 2000 cm^{-1}, on the final well side, if the electron has transferred, there can be degeneracy with, for different solvent configurations, different

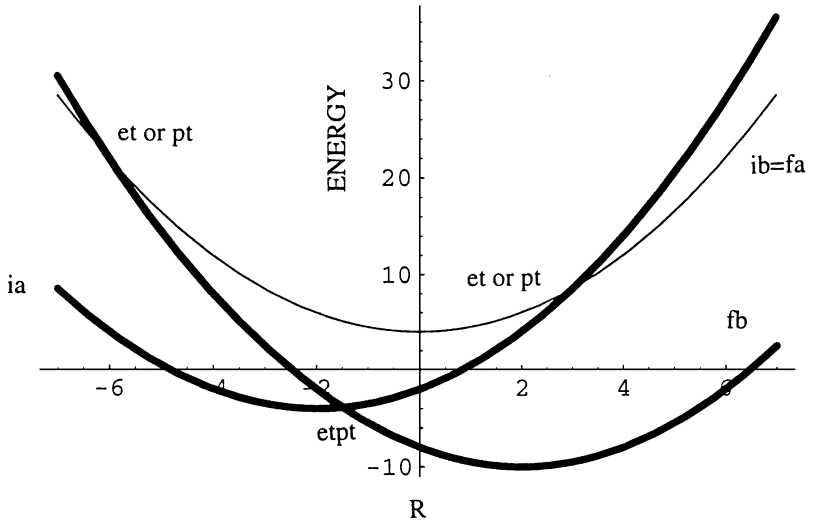

Figure 4 Diabatic surfaces for ET/PT and ETPT. ETPT is favored because the activation energy for crossing to the *f b* surface is essentially zero (activationless reaction) while ET (or PT) corresponds to continuing along the *R* coordinate to cross at the *fa* (or *ib*) surface.

proton final levels. Another solvent configuration could produce degeneracy with another final proton level. To appreciate this point, note that the scale of the solvent energetic fluctuations, which is essentially measured by the bandwidth parameter $\Delta = \sqrt{2\lambda_s k_B T} \sim 2000\ \text{cm}^{-1}$ for a λ_s of 1 eV, is consonant with the proton level separations (approximately the well frequency). Thus, the solvent fluctuations that drive the charge transfer can open up a number of channels for the different proton *a* and *b* states. In the picture presented above in Figures 3 and 4, there will be a manifold of surfaces for the *a* and *b* states, with the states in each manifold being separated by approximately the well frequency. The solvent coordinate picture analogous to Figure 2*b* then becomes as drawn in Figure 5. Then we can discuss ET/PT versus ETPT for each pair of crossing surfaces.

This putatively complicating feature, arising from the time scale (or mass) separation between the electron and the proton, suggests that a profitable approach would be to do a Born-Oppenheimer separation of the proton from the electron. That is, we should consider a restriction of the path in the 2D tunneling space as shown in Figure 6. The zigzag path expresses the feature that we may think of a 1D electron tunneling profile parametric on the proton's position. As the proton displaces, we assess the degeneracy for tunneling in the electron direction. Parametric on the solvent coordinate, the proton displaces until the electron's potential is symmetrized. Here, the electron may transfer

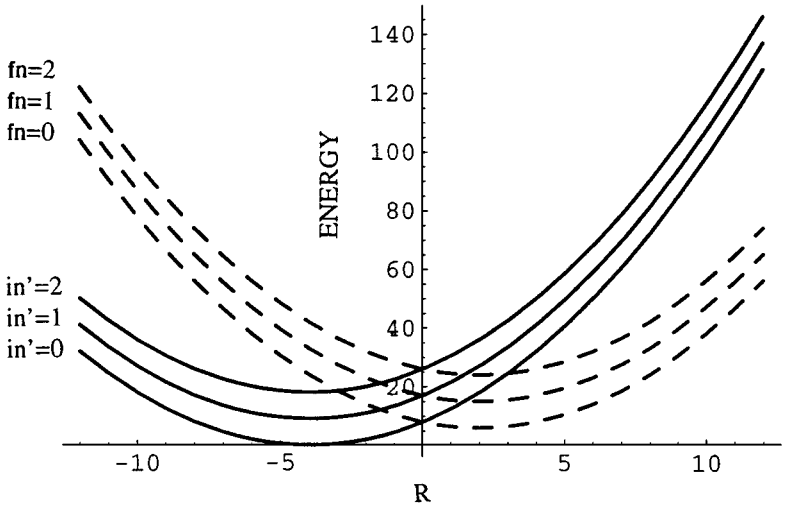

Figure 5 The proton provides a manifold (proton eigenstates, $n' = 0, 1, 2, \ldots$) of solvation surfaces with the electron in its initial state (*solid parabolas*) and a manifold (proton eigenstates, $n = 0, 1, 2, \ldots$) of solvation surfaces with the electron in its final state (*dotted parabolas*).

(with a probability dependent on the electronic coupling) and the proton may then either be modestly displaced but remain in its initial state or be displaced by a large amount and transfer to its final state.

A number of ways exist to obtain a 2D tunnel matrix element based on this restricted path. Perhaps the simplest method uses the BO scheme on the electron-proton wavefunctions $\Psi_i(r_e, r_p \mid R) = \Psi_i(r_e \mid R)\chi_{in'}(r_p \mid R)$ and $\Psi_f(r_e, r_p \mid R) = \Psi_f(r_e \mid R)\chi_{fn}(r_p \mid R)$ (11, 56, 57). We may view the ETPT process as driven by some residual coupling V_{res} and evaluate the matrix elements of this coupling between these states. By assuming that the matrix

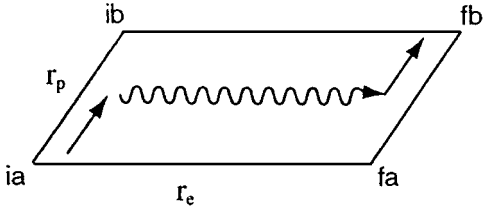

Figure 6 The path for 2D tunneling. *Wavy arrow* denotes electron tunneling when the proton rearranges to the proper configuration to symmetrize the electron PES. *Straight arrows* denote the proton motion for the initial *i* and final *f* electron states. The path is parametric on the solvent coordinate, *R*.

element can be factored according to

$$\begin{aligned} V_{etpt} &= \langle \Psi_i(r_e \mid R)\chi_{in'}(r_p \mid R)|V_{res}|\Psi_f(r_e \mid R)\chi_{fn}(r_p \mid R)\rangle \\ &\approx \langle \Psi_i(r_e \mid R)|V_{res}|\Psi_f(r_e \mid R)\rangle_{r_e}\langle \chi_{in'}(r_p \mid R)|\chi_{fn}(r_p \mid R)\rangle_{r_p} \\ &\equiv V_{el}\langle \chi_{in'}|\chi_{fn}\rangle \end{aligned} \quad 4.$$

and identifying the matrix element of the residual coupling with the electronic matrix element for electron transfer, we find the simple result that the ETPT coupling is the product of the ET electronic coupling and the Franck-Condon (FC) factors connecting the proton in its initial and final states. We have presented a formal derivation of this basic result (17).

Armed with this simplified coupling expression, we may consider a Golden Rule evaluation of the rate constant for ETPT where the coupling term is V_{etpt} and the reaction is driven by coupling to a solvent mode, R. The rate constant can be formulated as (17)

$$\begin{aligned} k_{ETPT} = \frac{V_{el}^2}{\hbar^2}\sqrt{\pi\hbar^2/\lambda_s^{ETPT}k_BT}\sum_{n'}\rho_{in'}\sum_{n\in b}|\langle\chi_{fn}\mid\chi_{in'}\rangle|^2 \\ \times e^{-\left(\lambda_s^{ETPT}+\Delta E^{el}+\varepsilon_{fn}-\varepsilon_{in'}\right)^2/4\lambda_s^{ETPT}K_BT}. \end{aligned} \quad 5.$$

Here, the equilibrium distribution of the proton, with the electron in its initial state, i, is $\rho_{in} = e^{-\beta\varepsilon_{in}}/Q$, with ε_{in} the energy levels of the proton in the reactant (a-state) well. In writing the reaction driving force $\Delta G^{(0)} = \Delta E^{el} + \varepsilon_{fn} - \varepsilon_{in'}$, we have split it up as ΔE^{el}, the electronic structure contribution, and $\varepsilon_{fn} - \varepsilon_{in'}$, the level difference of the proton in its b and a states, with the solvation contribution to these levels included in the definition of the vertical origin of the proton double well. When dealing with nonharmonic surfaces, this is a more convenient procedure, as the eigenstates are not equally spaced. Thus, the energy levels ε_{in} *and* ε_{fn} are referenced to the minima of their respective solvated proton potential energy surfaces $V_i(r_p)$ and $V_f(r_p)$.

The ETPT rate constant's form given in Equation 5 implies that it can be viewed as an ET rate constant driven by coupling to two nuclear modes: one, the solvent, treated classically, and the other, the proton, treated quantum mechanically (in terms of Franck-Condon factors). In fact, in another approach to ETPT that we referred to as the doubly adiabatic approach, if we assert that ETPT is an ET reaction with coupling to two modes—the solvent and an internal "vibrational" mode from the proton's displacement—then an ET Golden Rule calculation for an electron coupled to these two nuclear coordinates will lead to Equation 5 (17). A similar calculation was carried out in the context of hydrogen ion discharge, as noted in the Introduction (57). In this view, the

proton provides a *set* of solvation surfaces, as in Figure 5, for the proton in its manifold (n′) of initial, *a*, states and manifold (n) of final, *b*, states. The activation energies for each channel (each surface crossing) then reflects the conservation of energy requirement of the electron, the proton, and the solvent before and after charge transfer. The combination of proton-state–specific activation energy and proton FC factors comes from the combination of the classical solvent and quantum proton treatment. The doubly adiabatic scheme also makes it clear that if the proton does *not* transfer, then the electron transfer rate constant may be written as

$$k_{ET} = \frac{V_{el}^2}{\hbar^2}\sqrt{\pi\hbar^2/\lambda_s^{ET}k_BT}\sum_{n'}\rho_{in'}\sum_{n\in a}|\langle\chi_{fn}\,|\,\chi_{in'}\rangle|^2$$
$$\times\, e^{-\left(\lambda_s^{ET}+\Delta E^{el}+\varepsilon_{fn}-\varepsilon_{in'}\right)^2/4\lambda_s^{ET}K_BT}. \qquad 6.$$

The sum over final proton states, *n*, is now restricted to the reactant side, *a*, for the proton. The Franck-Condon factors for the proton then are "conventional" bond vibration ones. To the extent that there is a displacement of the origin of the proton vibration after ET, there will be Franck-Condon restrictions on the ET rate in addition to the solvation reorganization requirements. This expression is precisely what has been used for ET when there is a coupling to a low frequency (classical) mode and a high frequency (quantum) vibrational mode (73).

Finally, if we accept that there is a possibility of just proton transfer, and its mechanism is the same solvent symmetrizing one as for ET, then its rate constant can be written down in Golden Rule form as for ET in Equation 1, with all parameters now appropriate to the proton transfer reaction. Consonant with the idea of photochemical initiation of the reaction, this PT rate constant is appropriate to the charge distribution *after* ET. The electronic coupling for PT, V_{pt}, can be obtained by solving for the separation of the two lowest eigenvalues in the solvent symmetrized proton surface (with the electron in the *f* state).

We now have appropriate expressions for all the rate constants that describe the ET/PT and ETPT reaction channels. Before discussing how to evaluate the parameters that enter these expressions, let us compare the two mechanisms for kinetic efficiency. ET/PT is rate-limited, as the overall conversion rate constant satisfies

$$k^{-1} = k_{ET}^{-1} + k_{PT}^{-1}. \qquad 7.$$

Thus, if one step is slow, the overall conversion will not be rapid. ETPT by contrast is not rate-limited in this sense, but it is limited by the large tunneling path that must be involved. That is, if we view ETPT as a tunnel event that

takes place in the 2D space of the electron and proton coordinates, the tunnel path will be longer for ETPT versus separate ET or PT. This feature is readily apparent in Equation 5, where the large tunnel path for the zigzag approximation is manifest in the Franck-Condon factors. Because the *a* and *b* side FC factors are formed from wavefunctions whose origins are separated by the proton transfer distance, they can provide a severe constraint on the size of the ETPT rate constant. Note that it is imperative that these FC factors be evaluated by use of wavefunctions that properly reflect the geometry of the proton pes for the *i* and *f* electron states; a harmonic approximation to them would certainly tend to make these FC factors quite small. In the ET expression of Equation 6, the FC factors overlap proton wavefunctions on the (same) *a* side, so they are intrinsically larger than the ETPT FC factors.

EVALUATION OF PCET RATE CONSTANTS

Turning now to the evaluation of the parameters that enter the various rate constant expressions, as evident in Equations 5 and 6, what are needed, in part, are solvent reorganization energies, λ_s, and thermodynamic driving forces, $\Delta G^{(0)}$. A reorganization energy is the energetic cost of producing the equilibrium solvation of the product state when the solute charge distribution is initially appropriate to the reactant state. It is a nonequilibrium solvation property, because the initial Franck-Condon transition produces a solute charge state that is not in equilibrium with the solvent. The driving force is an equilibrium property and is more readily available experimentally than a reorganization energy. Both these energetics depend on the charge states of the reactants and products and their couplings to the solvent. Because the solute's charge states are different for the various intermediate and final states for the ET/PT versus the ETPT pathways, the corresponding energetics will differ and potentially lead to very different rate constants. Note that even though ET/PT is written as a consecutive expression in Equation 7, the PT reaction's energetics depend on the electron having transferred; in this sense, the PT reaction is not independent of the ET reaction. In addition to these solvation energetics, the proton FC factors must be evaluated.

A number of approaches can be used to obtain the required energetic quantities. The most straightforward is to use dielectric continuum methods, in the spirit of Marcus theory. This approach, although limited to regular geometries for the solute, is adequate for mapping out the contrasts between ET/PT and ETPT. Another potential methodology is via numerical solution of the Poisson-Boltzmann equation. It has been used to obtain equilibrium solvation energetics (driving forces) (74) for more complicated geometries. This method can also be used to evaluate reorganization energies (75). Molecular dynamics

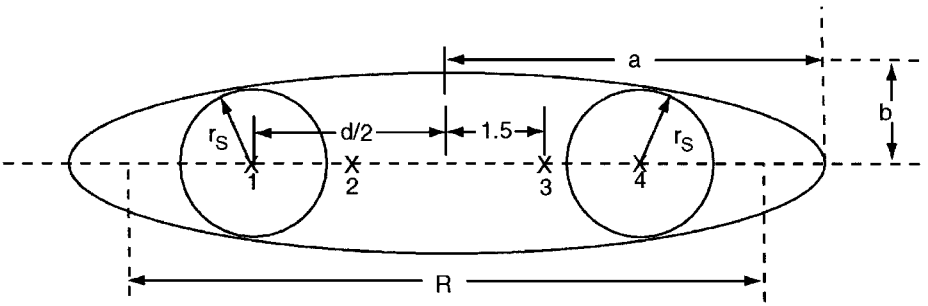

Figure 7 Model for the evaluation of the reorganization and solvation free energy of the ET, PT, and ETPT reactions. The donor and acceptor sites are spheres of radius r_s embedded in an ellipsoid with major (minor) axis a (b) and interfocal distance R. The locations 1 and 4 (2 and 3) denote charge sites associated with the electron (proton) states. The proton sites are at a fixed distance of 3 Å, and the electron sites are separated by a distance d of 15 Å. The ellipsoid expands to contain the donor and acceptor spheres as the sphere radii increase.

simulations can be used to obtain both driving force and reorganization energy, although to do this properly requires the use of solvents that are modeled as polar *and* polarizable (76, 77). We have done so for a model of symmetric ETPT in a simple polar/polarizable solvent model of dichloromethane (16). But such simulations in asymmetrical interfaces require knowledge of solvent potentials appropriate to a polar/polarizable solvent with intermolecular potentials between a (relatively large) solute in its possible charge states and the solvent. In the discussion below, we focus on the simplest method, dielectric continuum theory.

Figure 7 displays the model geometry we use to represent an electron donor and acceptor with its charge sites, labeled 1 and 4, and two interior charge sites, 2 and 3, for the hydrogen-bonded proton. The ellipsoid's dimension varies to accommodate the different sized spheres representing the electron donor and acceptor groups. Kirkwood & Westheimer (78–80) obtained an expression for $\Delta G^{(0)}$ for such ellipsoidal cavities, and Brunschwig et al (81) obtained the corresponding λ_s.

We may also use the Kirkwood & Westheimer (KW) method to obtain the proton-solvated surface as a function of the proton's coordinate. These surfaces, with the electron in its initial and final states, are required for the evaluation of the FC factors in Equations 5 and 6. We use a simple interpolation of charge (see below) to represent the change in the dipole moment of the hydrogen bonded complex as the proton transfers from the *a* to the *b* state. Parametric on the proton position in the hydrogen bond, we evaluate the solvation energy of the solute based on the KW expression for the instantaneous charge distribution of

the solute. The solvation energy to use here corresponds only to the electronic degrees of freedom of the solvent (the electronic polarization of the solvent). This solvation is the appropriate one to use, considering that it is fast with respect to the proton. We have extensively discussed the origin of this effect elsewhere (67). The KW $\Delta G^{(0)}$ corresponds to the energetic difference between the endpoints $r_p = r_{pb}$ and r_{pa} of the proton surface, where the full solvation, electronic and orientational, must be used.

APPLICATIONS

In this section, we present a selection of calculations on PCET that contrast the rates expected for the ET/PT and ETPT channels. The experimental data on PCET in the model asymmetrical and symmetrical hydrogen-bonded interfaces are summarized. The original theoretical (15–18) and experimental (19–24) references should be consulted for a more extensive presentation of results.

Pyridine-Pyridinium Hydrogen-Bonded Complexes

A prototypical example of a PCET reaction complex is a pyridine-pyridinium hydrogen bonded interface (18). Many such homoconjugated complexes have been studied spectroscopically to verify that the hydrogen-bonded proton can be characterized by a double well surface, as was inferred from electronic spectra that reflect the tautomeric equilibrium (82). The reactions can be schematized as

$$\mathrm{DN^+H{-}{-}NA^-} \leftrightarrow \mathrm{D^-N^+H{-}{-}NA} \quad ia \rightarrow fa \qquad \text{(ET)}$$
$$\mathrm{DN^+H{-}{-}NA^-} \leftrightarrow \mathrm{D^-N{-}{-}HN^+A} \quad ia \rightarrow fb \qquad \text{(ETPT)}$$

Scheme I

where D and A denote the electron donor and acceptor, respectively. (As written, the reactions are actually hole transfers, not electron transfers.) If the proton transfers, its state changes from *a* to *b*. The ETPT reaction is symmetric (so thermoneutral), while the ET reaction is not, because of the solvation effects. To obtain the solvated proton surfaces, the proton site charges are parametrized as $e_2(q) = 1-q$; $e_3(q) = q \quad 0 < q < 1$, where $q = (r_p - r_{p_a})/(r_{p_a} - r_{p_b})$ is a charging parameter that tracks the proton displacement in the interface in terms of the proton's *a*-state (r_{pa}) and *b*-state (r_{pb}) positions: in this case a linear charge change that models the hydrogen-bonded interface's dipole moment in the process $\mathrm{N^+{-}H{-}{-}N} \rightarrow \mathrm{N{-}{-}H{-}N^+}$. We find solvation energy differences between the initial charge distribution ($\mathrm{DN^+H{-}{-}NA^-}$), with a large dipole moment, and the smaller dipole state ($\mathrm{DN{-}{-}HN^+A^-}$), obtained by moving the proton across the hydrogen bond, of around 8-15 kcal/mol. The variation is due to different assumptions on the dimension of the ellipsoid chosen. A solvated proton surface is displayed in Figure 8. It is based on a proton gas phase surface

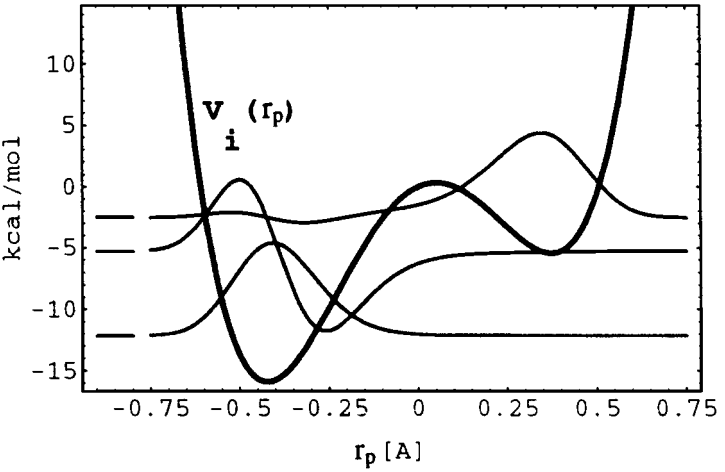

Figure 8 An *i* state proton surface that supports both ET and ETPT channels. The energies of the three proton localized levels are shown along with their corresponding wavefunctions. The corresponding pattern for the *f* state is obtained by inversion through the origin. In the initial state *i*, the lowest *a* (left-side-localized) proton state has good Franck-Condon overlap with the third (*a*-side) state of the *f* surface and can therefore permit a high ET rate constant.

that is represented by a quartic function with well frequency and well separation that provides a typical barrier for proton transfer. Table 1 lists representative parameters. Also shown are the proton wavefunctions and energies for the first three states.

By symmetry, the surface for the *f* state follows by inversion through the origin. These states and energies are obtained by numerical solution of the Schrödinger equation for the proton in the given potential surface. Knowledge of the proton wavefunctions for the initial and final electron states then permits numerical evaluation of the proton FC factors $\langle \chi_{in'} \mid \chi_{fn} \rangle$.

Table 1 Parameters used for the construction of the gas-phase proton surfaces

$(Q_b - Q_a)$ (Å)	$\bar{\omega}$ (cm^{-1})	V_{max} (cm^{-1})
0.5	2000	919
0.6	2200	1602
0.7	2200	2180
0.8	2500	3678

The Franck-Condon factors, the reorganization energies, and the energies of the localized states are used to calculate the ET and ETPT rate constants according to Equations 5 and 6. The final factor that enters these rate expressions is the ΔE^{el} that can arise from chemical differences in different Ds and As, or from a requirement that the charge transfer reaction be photochemically initiated. It does not alter the shape of the proton surfaces $V_{i,f}(r_p)$, at least for donors and acceptors that are reasonably electronically isolated from the hydrogen bonding interface.

Figure 9 displays the ETPT rate versus ΔE^{el} in order to exhibit deviations from a Marcus type of behavior. The characteristic maximum is found as in a Marcus plot, but the form is modulated by what amounts to a sum over Marcus plots that result from the different vibronic state contributions. If the vibronic states did correspond to oscillator states, and if there were no solvation effect from the proton displacement, then, as noted above, the rate expression would be the same as a two mode ET, with one mode treated classically, and the other quantum mechanically. Here, there is no possibility of ET, as the proton potential surface for the $i(f)$ electron state only allows for an $a(b)$ localized proton. The ETPT dependence on ΔE^{el} is similar to the parabolic form of Marcus ET theory, but the width of the parabola is not simply related to the solvent reorganization energy λ_s. The slower dependence (than for Marcus theory) on ΔE^{el} found for this particular case is typical of what we find for

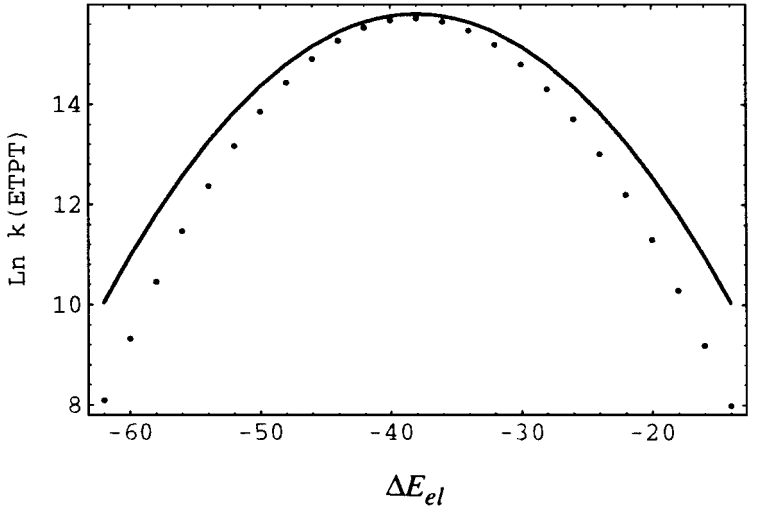

Figure 9 The log of the ETPT rate constant versus ΔE^{el}, the electronic driving force (—). *Dotted line*, plot of $\log(\lambda_s + \Delta E^{el})^2$ (what a one-mode Marcus parabola would yield).

Table 2 ETPT and ET rate constants for the NH^+N hydrogen-bonded interfaces

	$\bar{\omega}$ (cm^{-1})[a]									
	2000		2200		2500		$2000/\sqrt{2}$		$2200/\sqrt{2}$	
Solvation[b, d]	15.0	10.5	15.0	10.5	15.0	10.5	15.0	10.5	15.0	10.5
λ_s^{ETPT}[d]	32.3	48.8	32.3	48.8	32.3	48.8	32.3	48.8	32.3	48.8
λ_s^{ET}[d]					20.0	31.2				
k_{ETPT} (s^{-1})[c, d]	3.7E6	3.0E5	6.6E6	5.0E5	5.6E4		7.4E5	2.3E4	7.5E4	2.1E5
ΔE^{el}[d]	38.0	55.0	38.0	55.0	40.0		36.0	55.0	36.0	59.0
k_{ET} (s^{-1})[c, d]					2.4E8					
ΔE^{el}[d]					30.0					

[a]The other gas phase parameters for the proton surfaces are listed in Table 1.
[b]The solvation energy listed is the difference $G_f^{sol}(Q_b) - G_f^{sol}(Q_a) = -[G_i^{sol}(Q_b) - G_i^{sol}(Q_a)]$ for the *a* and *b* proton equilibrium states.
[c]The maximum rate as a function of ΔE^{el}.
[d]kcal/mol.

other rates obtained here, whether they are ET or ETPT channels. The maximum value of the rate constant is 3.7×10^6 sec^{-1} for $\Delta E^{el} = -38$ kcal/mol. The value of the rate constant is based on a V_{el} of 1 cm^{-1}. Because both the ET and ETPT rate constants are proportional to the square of V_{el} (cf Equations 5 and 6), the rate constants are readily compared for a uniform value of V_{el}.

In Table 2, we list the ETPT rate constants for several different double wells and solvation states. The solvation energy listed (first line of data in the table) is the difference: $G_f^{sol}(r_{p_b}) - G_f^{sol}(r_{p_u})$ for the proton equilibrium solvated states. The larger (smaller) solvation energy pertains to a smaller (larger) ellipsoid with electron D and A spheres of 3 (4) Å. The rates for the $\bar{\omega} = 2000$ cm^{-1} well are smaller than those for $\bar{\omega} = 2200$ cm^{-1}. The well with lower frequency has the wells closer and therefore the FC factors can be larger. But what is also crucial is the number of proton-localized levels supported by the potential. In these two cases there are two such levels.

The isotope effects obtained by replacing the interface proton by a deuteron tends to make the rate constant smaller. No systematic trend could be discerned. While the FC factors of course decrease with a heavier mass, the number of localized levels tends to increase, and it is the combination of the values and number of FC factors that determines the rate constant. For example, the weaker solvation pes for $\bar{\omega} = 2000/\sqrt{2}$ cm^{-1} supports 3 localized levels, while the corresponding strong solvation pes only supports 2. Thus, the weaker solvation rate is enhanced relative to the stronger solvation rate.

The $\bar{\omega} = 2500$ cm^{-1} case with the stronger solvation introduces the new feature of there also being an ET rate channel. This feature is readily appreciated

from examination of Figure 8. (Note that the $V_f(r_p)$ surface is related to the one displayed by inversion through the origin.) Now, there is the possibility of ET too, as the proton pes $V_f(r_p)$ has a sufficiently deep well on the high energy side to provide a *fa* state—the electron has transferred but the proton has not. The rate constant for this process can be larger than the ETPT rates because the Franck-Condon factor connecting the *ia* ($n = 1$) and *fa* ($n = 3$) states is close to unity. Note that both these proton states are "ground" states in their wells. (They would be ground states in the separated-well limit.)

The feature that the ET rate tends to be larger than the ETPT rate when both channels are possible is general. As discussed above, the ET rates do not have the FC "drag" that slows down the ETPT process. Of course, the energy mismatch of the levels also contribute to the rates' sizes. The ε_{in} and ε_{fn} reflect the solvation energetics and the proton gas phase surfaces and, in addition, the value of ΔE^{el} will contribute. Tuning the ΔE^{el} value, by chemical modification of the donor and/or acceptor, is the most effective means to emphasize one rate channel at the expense of the other.

Amidinium-Carboxylate Hydrogen-Bonded Interfaces

The amidinium-carboxylate hydrogen bonded interface, with flanking electron donors and acceptors, is an attractive interface for PCET studies. This interface models arginine-aspartate (Arg-Asp) salt bridges found to be important in many biological structures including RNA stem loops (83), zinc finger/DNA complexes (84, 85), and the active sites of dihydrofolate reductase (86), siroheme sulfite reductase (87), and cytochrome *c* oxidase (88, 89). But unlike the multiple guanidinium-carboxylate interactions of Arg-Asp, amidinium presents only one specific binding mode for carboxylate, thereby simplifying PCET studies. Moreover, the amidinium–carboxylate interface is exceptionally stable and association persists in solutions, even when the dielectric constant of the solvent is high. The high formation constants of the salt bridge agree well with Jorgensen's classification for two favorable secondary interactions composing the hydrogen-bonded interface (90, 91), bolstered by the stabilization imparted by the molecular recognition of the negatively charged carboxylate by the positively charged amidinium. The ability to efficiently construct the interface (20) on a variety of metal complex and porphyrin donors and acceptors affords a wide range of systems for PCET studies.

A direct experimental measure of the effect of the salt bridge on electron transfer is to undertake a comparative kinetics study of a donor—(amidinium-carboxylate)—acceptor complex and its switched interface donor—(carboxylate-amidinium)—acceptor congener. This study has been realized for a Ru(II) polypyridyl donor complex with the properly designed excited state structure and a 3,5-dinitrobenzene acceptor (24). The electron transfer reaction is initiated by laser excitation of the metal-to-ligand charge transfer (MLCT) transition

of the Ru(II) polypyridyl complex. In the absence of methyl substitution of the bipyridine (bpy) rings, the MLCT excited states involving the ancillary bpy and salt-bridged functionalized Mebpy are close in energy, and MLCT excitation removes the transferring electron from the PCET reaction pathway. Hence, a comparative PCET kinetics study is obscured by the possibility of transferring an electron from the ancillary bipyridine ligand in addition to the desired transfer of an electron from the carboxylate- or amidinium-derivatized bpy ligand (21). By tetramethylating the ancillary bpy ligands (tmbpy), the resulting tmbpy MLCT excited state is energetically destabilized by nearly 0.4 eV with regard to the MLCT excited states of Mebpy-amH^+ and Mebpy-COO^-. These MLCT energetics ensure that photoexcitation cleanly promotes the transferring electron on to the Mebpy ligand, from where it can smoothly advance to the dinitrobenzoic acceptor. As shown by the data in Table 3, in this case, the electron transfer rate within the Ru(II) polypyridyl donor—(carboxylate-amidinium)—dinitrobenzene acceptor assembly is $\sim 10^2$ faster than that for an assembly in which the interface is oriented in the opposite direction, Ru(II) polypyridyl donor—(amidinium-carboxylate)—dinitrobenzene acceptor(24).

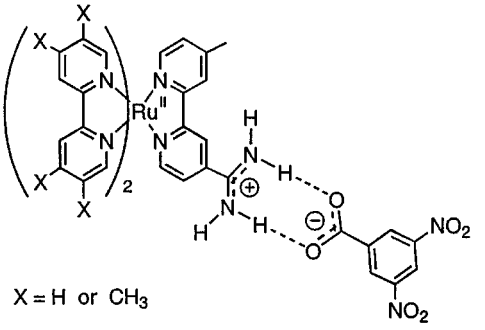

(1)

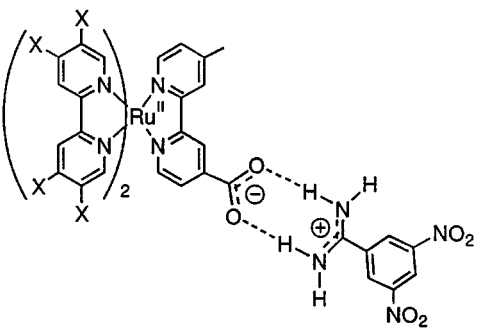

(2)

These differences in the rate for the "switched" interface systems offer interesting contrasts for the ET and ETPT rate constants. It is clear that the solvation energetics associated with the different possible charge states, the solvation of the proton's pes, and the gas phase pes can all depend on the interface's orientation.

There is the possibility, then, of differing rates for the two interface directions for the ET channel, and an analogous feature for the ETPT channel. The

Table 3 Rates for unimolecular and bimolecular electron transfer for donor-acceptor complexes with amidinium-carboxylate and dicarboxylic acid dimer bridges in dichloromethane at 22°C

Salt-bridge complex	ΔG°/eV	$k_{ET}/10^9$ M^{-1} s$^{(-1)a}$	$k_{PCET}/10^6$ s^b
1 (tmbpy) 2Ru(II)Mebpy-(amidinium-carboxylate)-(DNB)	−0.14	1.2	8.4
2 (tmbpy) 2Ru(II)Mebpy-(carboxylate-amidinium)-(DNB)	−0.34	3.3	310
3 (tmbpy) 2Ru(II)Mebpy-(COOH) 2-(DNB)	−0.23	3.2	43

[a]The bimolecular reaction of the respective constituents (nonhydrogen bonded) as determined by Stern-Volmer quenching kinetics.
[b]Unimolecular electron transfer of the salt-bridge associated donor-acceptor pair.

reactions for the four possibilities can be schematized as follows:

$$DO^-N^+A \rightarrow D^+O^-N^+A^- \quad (ET) \quad (1),$$
$$DO^-N^+A \rightarrow D^+ONA^- \quad (ETPT) \quad (2),$$
$$DN^+O^-A \rightarrow D^+N^+O^-A^- \quad (ET) \quad (3),$$
$$DN^+O^-A \rightarrow D^+NOA^- \quad (ETPT) \quad (4),$$

Scheme II

where we focus on the charge states for the four sites in the ellipsoid that define the interactions with the solvent. For example, in Reaction 4, the proton transfer neutralizes the charged interface as shown in Figure 1. The rate constants are constructed with the same considerations as outlined above for the

Table 4 Rate data for amidine–carboxylate hydrogen-bonded interfaces[a]

	$\bar{\omega}$ (cm^{-1})[a]							
DNOA interface	2500		2200		$2500/\sqrt{2}$		$2200/\sqrt{2}$	
k_{ETPT} (s^{-1})	6.0E1	0	0	0	0	0	0	0
ΔE^{el}	30							
k_{ET}	2.7E8	2.1E8	2.6E8	2.1E8	2.7E8	2.1E8	2.6E8	2.1E8
ΔE^{el}	40	60	40	60	40	62	44	64

	$\bar{\omega}$ (cm^{-1})[a]							
DONA interface	2500		2200		$2500/\sqrt{2}$		$2200/\sqrt{2}$	
k_{ETPT} (s^{-1})	7.1E6	4.1E6	1.8E6	5.1E6	7.1E2	7.6E3	1.0E6	4.1E4 (2.2E7)
ΔE^{el}	11	19	21	15	17	11	8	13 (9)
k_{ET} (s^{-1})	2.5E8	1.9E8	2.3E8	1.4E8	2.4E8	4.2E8	0.0	1.9E7 (0)
ΔE^{el}	5	13	9	15	3	11		11

[a]See legend to Table 2 for explanatory notes.

pyridine-pyridinium complexes. In Table 4, we display the rate constants for the DNOA (Scheme II, Reactions 1 and 2) and DONA interfaces (Scheme II, Reactions 3 and 4). Clearly, the different interfaces can have drastically different rates. Once again, we only present the maximum rate, obtained by varying ΔE^{el}. A behavior similar to that obtained in Figure 9 is observed for these interfaces. The data in Table 4 show that for the DNOA interface the ET channel is favored dramatically relative to ETPT. Essentially, the solvated PT surfaces show that there are no fb states available. The ET rates are quite large (for the chosen V_{el} of 1 cm^{-1}), because the reaction is essentially activationless. For the switched interface, the new solvated proton surfaces (we assume that the gas-phase surfaces are the same as for the DNOA interface) are quite different. They lead to stable fb states, corresponding to electron and proton transfer. For the displayed data, the ET rates are still larger than the ETPT rates, but again we have only listed the maximal rates. For other ΔE^{el} values, the ETPT rate can be larger than the ET rate.

The same methodology can be applied to amidinium-carboxylate interfaces that more closely mimic the experimental ones. However, a feature of the experimental solutes is that the D and A groups differ considerably in size, the acceptor being considerably smaller than the donor. We have still used the same ellipsoid models to investigate these reactions and can with reasonable parameters obtain trends observed in the rate data for the switched interface (18).

The electron transfer reaction associated with reductive quenching of electronically excited Ru(II) polypyridyl via the amidinium-carboxylate salt bridge has also been investigated. In this case, the PCET reaction effectively amounts to hole transfer from the Ru(II) metal center. Accordingly, the excited electron must be removed from the PCET pathway upon MLCT excitation, a situation that is achieved by modifying the ancillary bpy ligands with electron withdrawing diethylcarboxy (decb) groups (22):

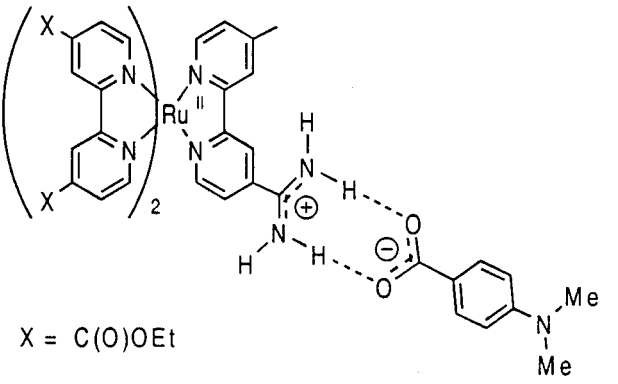

Electron transfer from a dimethylaniline donor into the Ru(II) metal center is fast [$k = 1.7(3) \times 10^9\ s^{-1}$] when the Ru(II) polypyridyl complex is attached to the amidinium-side of the salt bridge as opposed to the oxidative quenching reaction described above, where the fast electron transfer is observed for the Ru(II) polypyridyl complex attached to the carboxylate-side of the salt bridge. Notwithstanding, the results of the oxidative and reductive quenching pathways are parallel inasmuch as the fastest electron transfer is observed for ET (Reaction 1 of Scheme II), as opposed to an ET reaction (Reaction 3 of Scheme II), which may be stabilized by an ensuing proton transfer (Reaction 4 of Scheme II). For assemblies described by Reaction 1, the electron is transferred to a site already carrying the positive charge of the interface and proton transfer is not necessary for stabilization of the developing charge on the acceptor. Hence, Franck-Condon factors arising from proton motion within the salt bridge are minimized. Moreover, electron transfer is in the direction of the permanent dipole of the salt bridge in a D—(carboxylate-amidinium)—A orientation; the internal electric field therefore contributes favorably to the driving force of reaction relative to the isolated constituents (for which the redox potentials are measured). Thus, that the fastest ET rates occur for Reaction 1 appears to be a general result.

Carboxylate-Carboxylate Hydrogen-Bonded Interfaces

In contrast to salt bridge interfaces, proton motion within a charge-compensating interface does not lead to substantial changes in polarity, charge, and energetics of the electron transfer reaction. When proton motion leads to minimal charge redistribution within the interface, the perturbation of the proton on electron transport should be small. A photoinduced electron transfer reaction between a Zn(II) porphyrin donor and 3,4-dinitrobenzene acceptor bridged by a symmetric dicarboxylic acid interface exemplifies this type of PCET reaction. The rate constants for both charge separation and recombination of this donor/acceptor system were measured by picosecond transient absorption to be $5.0(5) \times 10^{10}\ s^{-1}$ and $1.0(2) \times 10^{10}\ s^{-1}$, respectively (19). That the rates are only slightly slower than those of covalently linked Zn(II) porphyrin/acceptor systems of similar separation and driving force (92) establishes that hydrogen bonded pathways for electron transfer can be competitive with covalent bond routes.

Because proton displacement on one side of the dicarboxylic acid interface is compensated by displacement of a proton from the other side, charge redistribution resulting from proton motion is minimized. The only mechanism available to engender PCET is the dependence of the electronic coupling on the position of the protons within the interface. Therien and coworkers attempted quantification of the coupling between an acceptor/donor pair through a dicarboxylic acid interface by using comparative kinetics measurements between a zinc(II)

porphyrin donor and an iron(III) porphyrin acceptor bridged by a dicarboxylic acid interface and the same donor-acceptor pair bridged by an interface composed of covalent carbon networks featuring the same number of bonds (93). A factor-of-two enhancement in the electron transfer rate constant when the donor-acceptor pair is bridged by the dicarboxylic acid interface has been attributed to greater electronic coupling modulated by a hydrogen-bond interface, as compared to a through-bond covalent carbon interface. However, considering the small difference in observed rate constants, this conclusion is compromised by the assumptions made in the determination of redox potentials, which were deduced from porphyrin precursors, as well as the possibility of energy transfer, which is typically significant for Zn(II)/Fe(III) porphyrin systems (94). The effect of the proton on the electronic coupling is revealed, however, in a deuterium isotope effect of the electron transfer rate constant. For the Zn(II) porphyrin donor–$(COOH)_2$–dinitrobenzene acceptor system, a pronounced deuterium isotope effect of $k_H/k_D = 1.7(3)$ and 1.6(4) for the charge separation and recombination rates, respectively, is observed.

We presented a theory of PCET (15) in symmetric proton interfaces that ascribes the coupling between the proton and electron to the dependence of the electronic coupling matrix element on the protons' positions in the interface, $V_{el} = V_{el}(r_p)$. The suggestion, verified by ab initio methods on a dicarboxylic acid dimer (16), was that $V_{el}(r_p)$ would maximize at the symmetric configuration of the protons in the interface. The major contributor to the increase in V_{el} was, in fact, the decrease in the O–O distance as the protons are moved from their equilibrium to the symmetric configuration. Bringing the flanking oxygens closer permits stronger electronic coupling. The modification to an ET rate constant resulting from this r_p dependence of electronic coupling can be viewed as a non-Condon effect on an ET rate constant. Its consequences to the rate-constant expression are the appearance of matrix elements of $V_{el}(r_p)$ between the protonic states in the protons' double well potential. Once $V_{el}(r_p)$ is known, and the eigenstates of the double-well proton potential are evaluated, the matrix elements can be obtained. The resulting PCET rate constant is about a factor of four larger than the standard ET rate constant that would be calculated by assuming that V_{el} is independent of the protons' position. It must be noted that there are several uncertainties in such a calculation. The ab initio methods required to evaluate the r_p dependence of V_{el} are not routine for a realistic system, and the double-well protonic potential surfaces for dicarboxylic acids are not known accurately. A way of minimizing the consequences of such uncertainties is to examine the isotope effect that would come from deuterating the interface protons. As the ET rate constant in this theory is dependent on the protonic matrix elements of $V_{el}(r_p)$, and replacing the protons by deuterons modifies these matrix elements, there will be an isotope effect on the PCET

rate constant. We found a range of values, $k_H/k_D \sim 1$–1.8, dependent on the assumed r_p dependence of $V(r_p)$. The heavier mass of the deuteron leads to a reduction of the rate constant relative to the proton rate constant, as found in the above experiments.

This diminished coupling of electron transport to proton motion found in the dicarboxylic acid studies is not restricted to symmetric interfaces. Results similar to that obtained for dicarboxylic acid interface systems are observed for acceptor-donor pairs juxtaposed by a complementary three-point guanine-cytosine interaction (95–98). Here, the pK_as of the bases can not accommodate proton transfer within the interface. As with the symmetric–$(COOH)_2$–interface, electron transport is facile over long distances, indicating little coupling of the interface to the electron transport.

CONCLUDING REMARKS

The focus of this review is on PCET where the electron and proton are intimately coupled. The examples we discussed from the realms of biology and materials were chosen to illustrate that this tight coupling can be an important mechanism for charge transfer. The introduction of model PCET systems with the electron donor and acceptor separated by a hydrogen-bonded interface presents an opportunity for a rigorous confrontation between experiment and theory. The well-defined, rigid geometry of the solutes that ensures intramolecular PCET limit the number of parameters that must be determined to predict a PCET rate constant. The charge changes resulting from switching the interface directions permit exploration of the large variations in the rate constants for the ET/PT versus ETPT reaction channels. And a further advantage of the porphyrin donor-acceptor systems with an amidinium or carboxylate in electronic communication with the pyrrole rings of the porphyrin is the possibility of timing the ET and PT rates independently. Specifically, salt-bridge formation engenders shifts of 5–10 nm in the Soret and Q-band spectral regions of the following porphyrin donor (23),

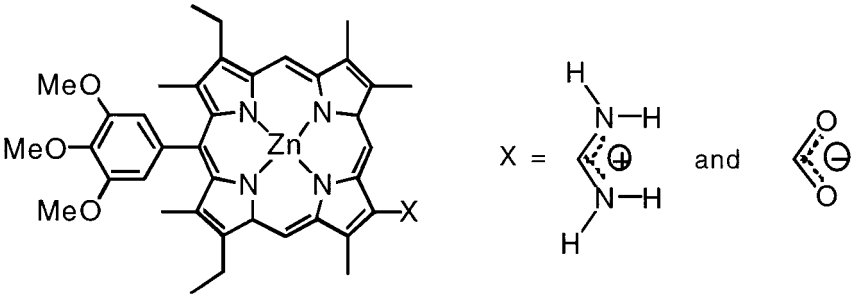

thus allowing the kinetics of the proton transfer events to be easily captured by time-resolved laser spectroscopy. Similarly, the corresponding electron transfer rate constants may be independently measured with the optical changes associated with the reduction of an appropriate acceptor.

Concerted ETPT was formulated as a 2D tunneling reaction driven by coupling to a solvent coordinate. The 2D ETPT derivation has the virtue of stressing the similar nature of the electron and proton as tunneling particles that should be simultaneously treated in a "first" Born-Oppenheimer equation sense. That is, the nuclear configuration of the solvent driving the charge transfer should be frozen, and the matrix element connecting the initial and final states of the process evaluated for this configuration. If the electron and proton were of comparable mass, then a genuine 2D tunneling problem would have to be addressed. It is the mass disparity that leads to the special zigzag path in the 2D tunnel space (cf Figure 6) and produces the seemingly different roles of the electron and proton, i.e. the electron transfers when the proton has displaced to a particular coordinate value. Furthermore, because the proton has a large mass relative to the electron, the proton's energy levels in the proton wells are comparable to the thermal energy bandwidth, and this leads to the involvement, in principle, of a manifold of proton states in the transfer process.

The theory of PCET that we summarized shows that the operational distinction between an ET (Equation 6) and an ETPT (Equation 5) rate constant is contained in a set of Franck-Condon factors. For ET, the FC factors refer to a proton that remains in its hydrogen-bonded state (*a* or *b* state) with a (small) displacement upon ET. Thus, the ET rate constant is appropriate to an ET reaction where there are two nuclear degrees of freedom driving the reaction; a solvation coordinate, treated classically, and a bond coordinate, treated quantum-mechanically. The PT rate constant may be assumed to be given by a similar nonadiabatic-based expression as for ET, with different parameters, of course. The overall PCET reaction then is rate-limited, as noted in Equation 7. For relatively low-barrier hydrogen bond potentials that can be present in some hydrogen bonded interfaces, the proton rate constant after ET could be quite large, and then the overall rate would be limited by the electron transfer rate constant.

For ETPT, the FC factors connect the proton wavefunctions in the initial (*a*) and final (*b*) states. Other things being equal, these FC factors tend to be smaller than those for a nontransferring proton. Therefore, ETPT rates can be limited by these small FC factors. Which reaction channel will actually dominate is sensitive to the solvation energetics corresponding to the various initial and final charge states, and the proton levels that are accessible to localized proton states, as indicated by the data in Tables 2 and 4.

The dielectric continuum methods used to evaluate the various solvation energetics required for the ET and ETPT rate constants are adequate to outline

the qualitative distinctions that arise for these reaction channels. However, the restriction to simple geometries for modeling the solutes is problematic. For a more quantitative comparison between theory and experiment, either Poisson-Boltzmann or molecular dynamics (MD) methods should be employed to obtain the solvation energetics. Work is now in progress to use MD to obtain the desired free and reorganization energies. Once MD is used to obtain solvation energetics, it can also be linked to the quantum-mechanical methods used to obtain the proton energy levels and wavefunctions required for the Franck-Condon factors. This can be accomplished by using the MD-generated solvent configurations to provide the solvation surfaces for the proton potential energy surfaces. When added to the gas-phase proton surfaces, the properly solvated proton surfaces are available, and they can be used to obtain the proton energies and wavefunctions.

ACKNOWLEDGMENTS

The authors gratefully acknowledge the financial support of the National Institutes of Health (GM 47274). Our thanks to Professor GT Babcock for many enjoyable discussions on various aspects of biological PCET.

Literature Cited

1. Okamura MY, Feher G. 1992. *Annu. Rev. Biochem.* 61:861–96
2. Takahashi E, Maroti P, Wraight C. 1992. In *Electron and Proton Transfer in Chemistry and Biology*, ed. A Muller, H Ratajczaks, W Junge, E Diemann, pp. 219–36. Amsterdam: Elsevier
3. Tommos C, Babcock GT. 1998. *Accts. Chem. Res.* 31:18–25
4. Ort DR, Yocum CF, eds. 1996. *Oxygenic Photosynthesis: The Light Reactions*, 4:213–47. Dordrecht, The Netherlands: Kluwer
5. Babcock GT, Wikström M. 1992. *Nature* 356:301–9
6. Link TA. 1992. In *Electron and Proton Transfer in Chemistry and Biology*, ed. A Muller, H Ratajczaks, W Junge, E Diemann, pp. 197–217. Amsterdam: Elsevier
7. Wikström M. 1998. *Biochim. Biophys. Acta.* In press
8. Malmström BG. 1993. *Acc. Chem. Res.* 26: 332–38
9. Ferguson-Miller S, Babcock GT. 1996. *Chem. Rev.* 96:2889–907
10. Marcus RA. 1964. *Annu. Rev. Phys. Chem.* 15:155–96
11. Ulstrup J. 1979. *Charge Transfer Processes in Condensed Media*. Berlin: Springer-Verlag
12. Birge RR. 1990. *Annu. Rev. Phys. Chem.* 41:683–733
13. Durr H, Bouas-Laurent H. 1990. *Photochromism: Molecules and Systems. Studies in Organic Chemistry 40*. Amsterdam: Elsevier
14. Scherl M, Haarer D, Fischer J, DeCian A, Lehn J-M, Eichen Y. 1996. *J. Phys. Chem.* 100:16175–86
15. Cukier RI. 1994. *J. Phys. Chem.* 98:2377–81
16. Zhao XG, Cukier RI. 1995. *J. Phys. Chem.* 99:945–54
17. Cukier RI. 1995. *J. Phys. Chem.* 99:16101–15
18. Cukier RI. 1996. *J. Phys. Chem.* 100: 15428–43
19. Turro C, Chang CK, Leroi GE, Cukier RI, Nocera DG. 1992. *J. Am. Chem. Soc.* 114:4013–15

20. Kirby JP, van Dantzig NA, Chang CK, Nocera DG. 1995. *Tetrahedron Lett.* 36:3477–80
21. Roberts JA, Kirby JP, Nocera DG. 1995. *J. Am. Chem. Soc.* 117:8051–52
22. Roberts JA, Kirby JP, Wall ST, Nocera DG. 1997. *Inorg. Chim. Acta* 263:395–405
23. Deng Y, Roberts JA, Peng SM, Chang CK, Nocera DG. 1997. *Angew. Chem. Int. Ed. Engl.* 36:2124–27
24. Kirby JP, Roberts JA, Nocera DG. 1997. *J. Am. Chem. Soc.* 119:9230–36
25. Wikström M. 1989. *Nature* 338:776–78
26. Mitchell P. 1961. *Nature* 191:144–48
27. Maroti P, Wraight CA. 1990. In *Current Research in Photosynthesis*, ed. M Baltscheffsky, 1:165–68. Dordrecht: Kluwer
28. Wraight CA. 1979. *Biochim. Biophys. Acta* 548:309–27
29. Okamura MY, Feher G. 1995. In *Anoxygenic Photosynthetic Bacteria*, ed. RE Blankenship, MT Madigan, CE Bauer, pp. 577–94. Dordrecht: Kluwer
30. Takahashi E, Wraight CA. 1992. *Biochemistry* 31:855–66
31. Paddock ML, Rongey SH, McPherson PH, Juth A, Feher G, Okamura MY. 1994. *Biochemistry* 33:734–45
32. McPherson PH, Schönfeld M, Paddock ML, Okamura MY, Feher G. 1994. *Biochemistry* 33:1181–93
33. Graige MS, Paddock ML, Bruce JM, Feher G, Okamura MY. 1996. *J. Am. Chem. Soc.* 118:9005–16
34. Meyer B, Schlodder E, Dekker JP, Witt HT. 1989. *Biochim. Biophys. Acta* 974:36–43
35. Bögerhausen O, Haumann M, Junge W. 1996. *Ber. Bunsenges. Phys. Chem.* 100: 1987–92
36. Ahlbrink R, Haumann M, Cherepanov D, Bögershausen O, Mulkidjanian A, Junge W. 1998. *Biochemistry* 37:1131–42
37. Lavergne J, Junge W. 1993. *Photosyn. Res.* 38:279–96
38. Hoganson CW, Babcock GT. 1997. *Science* 277:1952–56
39. Tommos C, Tang X-S, Warncke K, Hoganson CW, Styring S, et al. 1995. *J. Am. Chem. Soc.* 117:10325–35
40. Brudvig GW. 1992. *Acc. Chem. Res.* 24:311–16
41. Vincent JB, Christou G. 1989. *Adv. Inorg. Chem.* 33:197–257
42. Pecoraro VL. 1992. *Manganese Redox Enzymes*. New York: VCH
43. Roecker L, Meyer TJ. 1987. *J. Am. Chem. Soc.* 109:746–54
44. Geselowitz D, Meyer TJ. 1990. *Inorg. Chem.* 29:3894–96
45. Binstead RA, Meyer TJ. 1987. *J. Am. Chem. Soc.* 109:3287–97
46. Binstead RA, McGuire ME, Dovletoglou A, Seok WK, Roecker LE, Meyer TJ. 1992. *J. Am. Chem. Soc.* 114:173–86
47. Blair DF, Ellis WR Jr, Wang H, Gray HB, Chan SI. 1986. *J. Biol. Chem.* 261:11524–37
48. Kitagawa T, Ozura T. 1997. *Prog. Inor. Chem.* 45:431–79
49. Atherton SJ, Harriman A. 1993. *J. Am. Chem. Soc.* 115:1816–22
50. Shafirovich VY, Courtney SH, Ya NQ, Geacintov NE. 1995. *J. Am. Chem. Soc.* 117:4920–29
51. Gust D, Moore TA, Moore AL, Barrett D, Harding LO, et al. 1988. *J. Am. Chem. Soc.* 110:321–23
52. Gust D, Moore TA, Moore AL, Gao F, Luttrull D, et al. 1991. *J. Am. Chem. Soc.* 113:3638–49
53. Gust D, Moore TA, Moore AL. 1993. *Acc. Chem. Res.* 26:198–205
54. Hung S-C, Macpherson AN, Lin S, Liddell PA, Seely GR, et al. 1995. *J. Am. Chem. Soc.* 117:1657–58
55. Krishtalik LI. 1970. *Adv. Electrochem. Electrochem. Eng.* 7:283–339
56. Levich VG. 1970. In *Physical Chemistry—An Advanced Treatise*, ed. H Henderson, W Yost, 9B:985–1074. New York: Academic
57. Benderskii VA, Grebenshchikov SY. 1994. *J. Electroanal. Chem.* 375:29–44
58. Felderhoff M, Steller I, Reyes-Arellano A, Boese R, Sustmann R. 1996. *Adv. Mater.* 8:402–5
59. Nakasuji K, Sugiura K, Kitagawa T, Toyoda J, Okamoto H, et al. 1991. *J. Am. Chem. Soc.* 113:1862–64
60. Newton MD, Sutin N. 1984. *Annu. Rev. Phys. Chem.* 35:437–80
61. Closs GL, Miller JR. 1988. *Science* 240:440–47
62. Winkler JR, Gray HB. 1992. *Chem. Rev.* 92:369–79
63. Marcus RA. 1956. *J. Chem. Phys.* 24:979–89
64. Marcus RA, Sutin N. 1985. *Biochim. Biophys. Acta* 811:265–322
65. Formosinho SJ, Arnaut LG. 1993. *J. Photochem. Photobiol. A* 75:21–48
66. Marcus RA. 1975. *Faraday Symp. Chem. Soc.* 10:60–68
67. Cukier RI, Zhu J. 1997. *J. Phys. Chem.* 101:7180–90
68. Marcus RA. 1956. *J. Chem. Phys.* 24:966–78
69. Zeeger-Huyskens T, Huyskens P. 1980. In *Molecular Interactions*, ed. H Ratajczak, WJ Orville-Thomas, 2:1–106. New York: Wiley

70. Fang J-Y, Hammes-Schiffer S. 1997. *J. Chem. Phys.* 106:8442–54
71. Fang J-Y, Hammes-Schiffer S. 1997. *J. Chem. Phys.* 107:5727–39
72. Fang J-Y, Hammes-Schiffer S. 1997. *J. Chem. Phys.* 107:8933–39
73. Kestner NR, Jortner J, Logan J. 1974. *J. Phys. Chem.* 78:2148–66
74. Honig B, Nicholls A. 1995. *Science* 268: 1144–49
75. Simonson T, Perahia D. 1995. *J. Am. Chem. Soc.* 117:7987–8000
76. Warshel A, Levitt M. 1976. *J. Mol. Biol.* 103:227–49
77. King G, Warshel A. 1990. *J. Chem. Phys.* 93:8682–92
78. Kirkwood JG, Westheimer FH. 1938. *J. Chem. Phys.* 6:506–12
79. Kirkwood JG, Westheimer FH. 1938. *J. Chem. Phys.* 6:513–17
80. Kirkwood JG, Westheimer FH. 1939. *J. Chem. Phys.* 7:437
81. Brunschwig BS, Ehrenson S, Sutin N. 1986. *J. Phys. Chem.* 90:3657–68
82. Rabold A, Bauer R, Zundel G. 1995. *J. Phys. Chem.* 99:1889–95
83. Puglisi JD, Chen L, Frankel AD, Williamson JR. 1993. *Proc. Natl. Acad. Sci. USA* 90:3680–84
84. Berg JM. 1995. *Acc. Chem. Res.* 28:14–19
85. Pavletich NP, Pabo CO. 1991. *Science* 252:809–17
86. Howell EH, Villafranca JE, Warren MS, Oatley SJ, Kraut J. 1986. *Science* 231:1123–28
87. Crane BR, Siegel LM, Getzoff ED. 1995. *Science* 270:59–67
88. Ramirez BE, Malmström BG, Winkler JR, Gray HB. 1995. *Proc. Natl. Acad. Sci. USA* 92:11949–51
89. Brzezinski P. 1996. *Biochemistry.* 35: 5611–15
90. Pranata J, Wierschke SG, Jorgensen WL. 1991. *J. Am. Chem. Soc.* 113:2810–19
91. Jorgensen WL, Pranata J. 1990. *J. Am. Chem. Soc.* 112:2008–10
92. Wasielewski MR, Niemczyk MP, Svec WA, Pewitt EB. 1985. *J. Am. Chem. Soc.* 107:1080–82
93. DeRege PJF, Williams SA, Therien MJ. 1995. *Science* 269:1409–13
94. McLendon G, Winkler JR, Miller JR, Nocera DG, Mauk MR, Mauk AG. 1985. *J. Am. Chem. Soc.* 107:739–40
95. Sessler JL, Wang B, Harriman A. 1993. *J. Am. Chem. Soc.* 115:10418–19
96. Harriman A, Kubo Y, Sessler JL. 1992. *J. Am. Chem. Soc.* 114:388–90
97. Berman A, Izraeli ES, Levanon H, Wang B, Sessler JL. 1995. *J. Am. Chem. Soc.* 117:8252–57
98. Sessler JL, Wang B, Springs SL, Brown CT. 1997. In *Comprehensive Supramolecular Chemistry*, ed. Y Murakami, 4:311–36. Oxford, UK: Pergamon

Annual Review of Physical Chemistry
Volume 49, 1998

CONTENTS